

AWARD NUMBER: W81XWH-15-1-0110

TITLE: Noninvasive Characterization of Indeterminate Pulmonary Nodules Detected on Chest High-Resolution Computed Tomography

PRINCIPAL INVESTIGATOR: Fabien Maldonado

CONTRACTING ORGANIZATION: Vanderbilt University
Nashville, TN 37240

REPORT DATE: October 2016

TYPE OF REPORT: Annual

PREPARED FOR: U.S. Army Medical Research and Materiel Command
Fort Detrick, Maryland 21702-5012

DISTRIBUTION STATEMENT: Approved for Public Release;
Distribution Unlimited

The views, opinions and/or findings contained in this report are those of the author(s) and should not be construed as an official Department of the Army position, policy or decision unless so designated by other documentation.

REPORT DOCUMENTATION PAGE		<i>Form Approved</i> <i>OMB No. 0704-0188</i>
<small>Public reporting burden for this collection of information is estimated to average 1 hour per response, including the time for reviewing instructions, searching existing data sources, gathering and maintaining the data needed, and completing and reviewing this collection of information. Send comments regarding this burden estimate or any other aspect of this collection of information, including suggestions for reducing this burden to Department of Defense, Washington Headquarters Services, Directorate for Information Operations and Reports (0704-0188), 1215 Jefferson Davis Highway, Suite 1204, Arlington, VA 22202-4302. Respondents should be aware that notwithstanding any other provision of law, no person shall be subject to any penalty for failing to comply with a collection of information if it does not display a currently valid OMB control number. PLEASE DO NOT RETURN YOUR FORM TO THE ABOVE ADDRESS.</small>		
1. REPORT DATE October 2016	2. REPORT TYPE Annual	3. DATES COVERED 30 Sep 2015 - 29 Sep 2016
4. TITLE AND SUBTITLE Noninvasive Characterization of Indeterminate Pulmonary Nodules Detected on Chest High-Resolution Computed Tomography		5a. CONTRACT NUMBER
		5b. GRANT NUMBER W81XWH-15-1-0110
		5c. PROGRAM ELEMENT NUMBER
		5d. PROJECT NUMBER
6. AUTHOR(S) Fabien Maldonado E-Mail: Fabien.maldonado@vanderbilt.edu		5e. TASK NUMBER
		5f. WORK UNIT NUMBER
7. PERFORMING ORGANIZATION NAME(S) AND ADDRESS(ES) Vanderbilt University Medical Center 3319 West End Ave, STE. 910 Nashville, TN 37203		8. PERFORMING ORGANIZATION REPORT NUMBER
9. SPONSORING / MONITORING AGENCY NAME(S) AND ADDRESS(ES) U.S. Army Medical Research and Materiel Command Fort Detrick, Maryland 21702-5012		10. SPONSOR/MONITOR'S ACRONYM(S)
		11. SPONSOR/MONITOR'S REPORT NUMBER(S)
12. DISTRIBUTION / AVAILABILITY STATEMENT Approved for Public Release; Distribution Unlimited		
13. SUPPLEMENTARY NOTES		

14. ABSTRACT

Purpose: Lung cancer is the most common cause of cancer-related deaths in the US. Results from the National Lung Screening Trial (NLST), a large randomized controlled trial, suggest that screening with annual low-dose, high-resolution computed tomography of the chest (HRCT) reduces lung cancer specific mortality by 20%. The major challenge for the implementation of lung cancer screening is the high false positive rate. In the NLST, 40% of the participants in the HRCT were found to have lung nodules, 95% of which proved benign. This high false positive rate limits the applicability of this strategy at the population level, and could result in increased patient anxiety, radiation exposure, health care costs, and procedural morbidity and mortality. Our work aims at identifying HRCT-based and clinical variables to derive a model which will non-invasively distinguish benign from malignant nodules.

Scope: Based on our prior data on HRCT-based quantitative imaging, we are currently developing a multivariate radiologic prediction model (radiologic model) using a population of benign and malignant lung nodules identified in the NLST dataset. Epidemiologic and clinical variables from the same individuals will then be included to develop a multivariate combined clinical/radiologic model. We will then validate these models on the prospective study Detection of Early lung Cancer Among Military Personnel Study 1 (DECAMP-1).

Major findings: 657 nodules measuring between 8 and 30 mm with HRCT suitable for volumetric quantitative analysis were identified from the NLST dataset and included 338 malignant and 319 benign nodules. Datasets were transferred from the NLST image repository and transferred to Mayo Clinic for nodule identification and segmentation. Multiple candidate metrics were developed and considered for their ability to distinguish benign from malignant nodules, and their performance was analyzed by receiver operative characteristic curve analysis (see accomplishments section). Multivariate logistic regression, linear/quadratic discriminant analysis

15. SUBJECT TERMS

16. SECURITY CLASSIFICATION OF:			17. LIMITATION OF ABSTRACT UU	18. NUMBER OF PAGES 28	19a. NAME OF RESPONSIBLE PERSON USAMRMC
a. REPORT U	b. ABSTRACT U	c. THIS PAGE			19b. TELEPHONE NUMBER (include area code)

Standard Form 298 (Rev. 8-98)
Prescribed by ANSI Std. Z39.18

Table of Contents

	<u>Page</u>
Introduction.....	5
Keywords.....	5
Accomplishments.....,	5
Impact.....	25
Changes/Problems.....	26
Products.....	27
Participants & Other Collaborating Organizations.....	28
Special Reporting Requirements.....	N/A
Appendices.....	N/A

1. INTRODUCTION:

Lung cancer accounts for more cancer-related deaths in the US than colon, prostate and breast cancer combined, approximately 160,000 deaths per year. In 2011, a large randomized controlled trial, the National Lung Screening Trial (NLST) demonstrated a 20% relative reduction in lung cancer mortality with annual low-dose chest computed tomography (LD-CT). These encouraging results have led to widespread endorsement of lung cancer screening, but at the cost of identifying many false-positive LD-CT. In the NLST, 40% of patients had identifiable lung nodules, 96% of which proved benign. The ever-expanding use of chest CT in the US (estimated 20 million/year) is contributing to the identification of an estimated 1.5 million new nodules every year. Novel tools to distinguish benign from malignant nodules are urgently needed. We have previously demonstrated that volumetric CT-based quantitative characterization of lung nodules belonging to the adenocarcinoma spectrum is useful in risk-stratifying these lesions, exploiting the wealth of data points available with modern CT imaging. In this project, we are attempting to use similar quantitative imaging metrics to assist radiologists and clinicians in determining the likelihood of malignant nodule based on radiologic (radiologic model) and combined clinical and radiologic characteristics (clinical-radiologic model). To do so, we are using the available NLST dataset as a training set and have secured access to the large ongoing prospective study Detection of Early lung Cancer Among Military Personnel Study 1 (DECAMP-1). This project, if successful, will help to limit morbidity, mortality and healthcare costs associated with the management of incidentally or screen-identified pulmonary nodules.

2. KEYWORDS:

lung adenocarcinoma – overdiagnosis – Lung cancer screening – chest computed tomography – biomarkers – lung nodules.

3. ACCOMPLISHMENT:

1. What were the major goals of the project?

Aim 1 (first year of the grant): The first aim of this grant was to develop an imaging-based approach using volumetric analysis of screen-identified lung nodules, and a combined clinical-radiologic model to differentiate benign from malignant nodules.

- a. Milestone: Development of optimized quantitative radiological variables predictive of the benign or malignant character of lung nodules from a cohort isolated from the NLST (12 months – October 2016).

Note that subcontracts with Brown University and Mayo Clinic (required due to relocation of the PI, Fabien Maldonado, to Vanderbilt University) were not established until March 2016 and as such work could not be started before that time.

The identification of optimized quantitative radiological variables is 90% complete (see section 2).

- b. Milestone: development of a radiologic prediction model (12 months)

The radiologic model is contingent upon all optimized quantitative radiological variables being finalized and has not been started yet.

- c. Development of a combined clinical/radiologic prediction model (12 months).

The clinical/radiologic model is contingent upon all optimized quantitative radiological variables being finalized and has not been started yet. Clinical variables are available from the NLST database (see below)

Aim 2 (second year of the grant): the second aim of this grant is to prospectively validate the models developed in Aim 1 in the DECAMP-1 dataset (500 patients with indeterminate pulmonary nodules, DECAMP PROTOCOL ACRIN 4703).

Milestone: Validation of a radiologic and combined clinical/radiologic prediction models (**Year 2 of the grant**).

This work has not been started yet.

2. What was accomplished under these goals:

Major activities:

2.1 NLST Case selection and image transfer:

NLST Subject Selection

Four groups of participants were selected from the pool of eligible participants, who did not withdraw from follow-up, in the CT arm of the NLST (N=26,262).

The four groups are (1) screen-detected Lung cancer cases of the type adenocarcinoma and BAC, (2) non-lung cancer controls, (3) screen-detected lung cancer controls which includes squamous cell carcinomas, large cell carcinomas, small cell carcinomas and carcinoids and (4) an additional set of non-lung cancer controls where the nodule size was larger than 7mm. Groups (1) and (2) were selected initially and groups (3) and (4) were selected subsequently.

- (1) All screen-detected lung cancer cases of the type adenocarcinoma and BAC identified in the pool defined above were identified (N=342; 40% ACRIN, 60% LSS).
- (2) Non-lung cancer controls were selected as a stratified random sample from all participants in the pool defined above who were not found to have lung cancer during the screen or follow-up periods of the NLST and additionally only had one type of nodule identified on the CT image where a nodule was first identified. Participants were then stratified based on study arm and nodule type to create 6 strata; the two study groups by the three nodule types (solid, ground glass and part-solid). 770 non-lung cancer controls were to be selected is based on a 2:1 ratio with the lung cancer cases, with a 10% attrition rate for images not available. We stratified by study based on the percent of cases identified and by nodule based on an even split within each study. LSS for each nodule

type was 154, ACRIN for each nodule type was 103 resulting 771 non-lung cancer controls total identified. For each stratum a simple random sample based on the univariate distribution was used to select the controls.

- (3) All screen-detected lung cancer cases of the type squamous cell carcinomas, large cell carcinomas, small cell carcinomas and carcinoids were identified in the pool defined above (N=218; 37% ACRIN, 63% LSS).
- (4) An additional 40 non-lung cancer controls were selected as a stratified random sample from all participants in the pool defined above who were not originally selected in group 2 and using the same criteria as group 2, resulting in 16 ACRIN and 32 LSS participants. Note of the original group 2 (only 362 are within the limits of 7 – 30 mm in size for the nodules).

After all cases and non-LC controls were identified for groups 1 and 2 (N=1113). Case lists were prepared and sent to the LSS and ACRIN core labs to identify images to send. The core labs informed us that 10 images were unavailable resulting in 1103 cases available for groups 1 and 2. These 1103 were stratified by case status (case versus control) and for the controls by nodule type and randomly split into two data sets, training and validation.

A case list for LC-controls were prepared and sent to the core labs (N=218). The core labs informed us that 5 images were unavailable resulting 213 cases available for group 3. These 213 were randomly split into two data sets, training and validation.

A case list for the additional non-LC controls (N=40) was prepared and sent to the LSS core lab to identify images to send. All 40 had available images.

Image transfer

1. From LSS Core Lab

After receiving the list of participant identification numbers for the desired population of CT images, LSS Core Lab transmitted the list to the NLST data managers for linking to image identifiers. The image identifiers were then transmitted to the Cancer Imaging Archive (TCIA).

After the image verification, the investigators were required to ship a hard drive to TCIA. Staff at TCIA copied the selected CT images to the hard drive. The drive was then shipped back to the investigators.

2. From ACRIN Imaging Core Lab

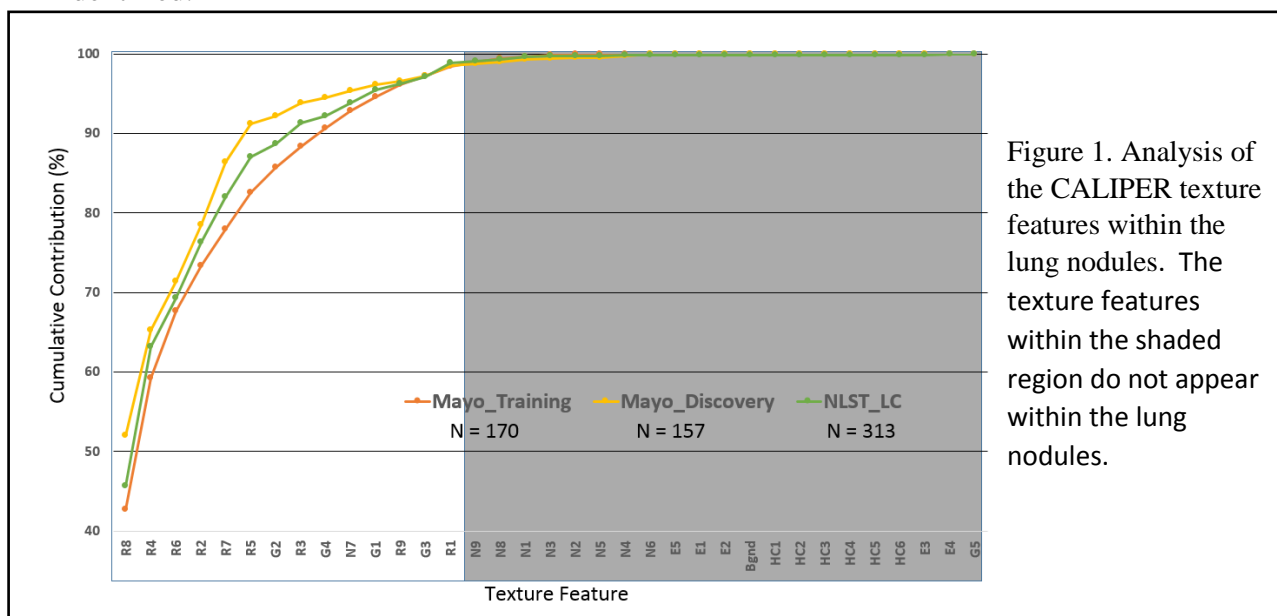
Three processes were used at the ACRIN Core Lab to deliver the required images to the investigators.

- A) On their initial request, the investigators were given a secure hard drive that contained images that they requested to begin their analysis right away.
- B) After the investigators had TRIAD set up on their system, the subsequent imaging data was made available to the investigators on a folder that only each individual can access.
- C) For small amount of image data, an SFTP account was created to deliver the images to the investigators.
- D)

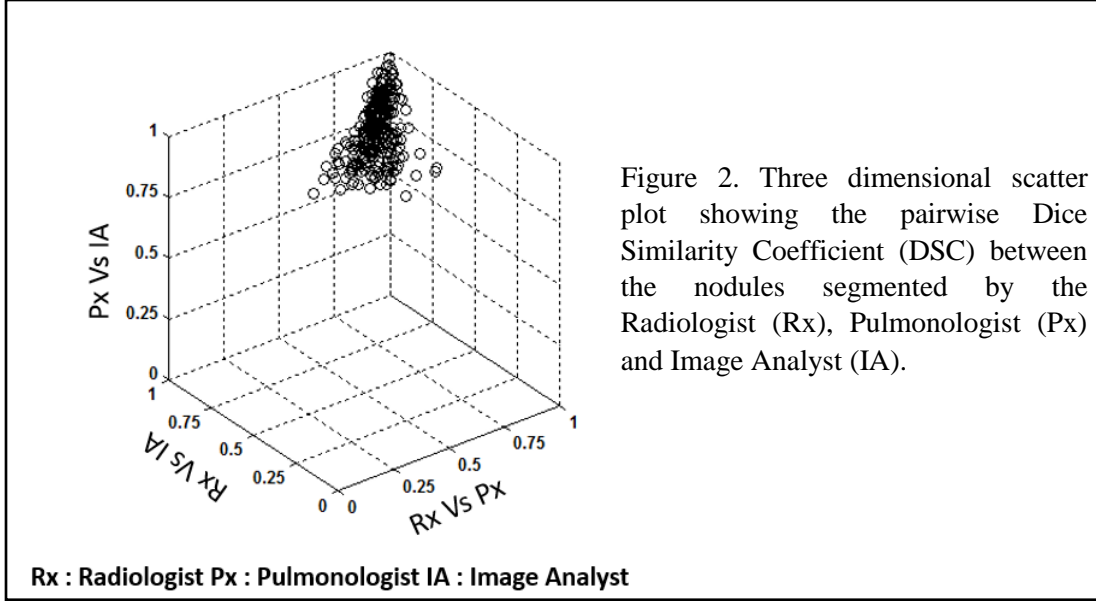
2.2 Development and optimization of quantitative radiological variables:

The following tasks were accomplished towards the identification and optimization of quantitative radiological variables to enable the differentiation of benign and malignant lung nodules :

2.2.1 Optimization and validation of nodule segmentation. For the feasibility pilot study, the lung nodules were segmented manually using ANALYZE software (Biomedical Imaging Resource, Mayo Clinic, Rochester, MN). The location and the extent of each nodule was identified visually and a stack of two dimensional borders were traced out along the transverse orientation. Tracing errors were minimized by guiding the manual traces along the automatically detected edges. Apart from being intensive and subjective, the manual approach suffers from out-of-plane discontinuities arising due to section-by-section two dimensional delineation of a three dimensional object. Towards optimizing the nodule segmentation, we developed a semi-automatic region growing approach based on the operator specified bounding cube enclosing the nodule and a seed location within the nodule. Manual editing tools were added to remove, if needed, intruding structures like vessels and pleura. Region growing approaches traditionally use the underlying voxel intensities to identify and agglomerate regions similar to the intensity at the seed location. Such an approach is highly sensitive to placement of the seed and the inherent noise in the scan. We developed a “parametric” feature-based region growing technique based on the texture classification of the voxels within the operator specified bounding cube. The texture classification is based on CALIPER software (Mayo Clinic, Rochester, MN). The detection and quantification of pulmonary parenchyma on CT scans by CALIPER (Computer Aided Lung Informatics for Pathology Evaluation and Rating) is based on histogram signature mapping techniques trained through expert radiologist consensus assessment of pathologically confirmed training sets. Using CALIPER, we analyzed the signatures of a multitude of manually segmented nodules derived from the Mayo training, discovery and NLST lung cancer cohort (Figure 1). Through this exercise, the candidate texture features for the parametric region growing were identified.



Towards validating the reproducibility and repeatability of the proposed segmentation, three operators (experienced radiologist, pulmonologist and image analyst) segmented multiple nodules ($N = 266$) from the NLST Controls cohort. The segmentation masks generated by the operators were compared pairwise using Dice Similarity Coefficient (DSC; Figure 2). The 95% CI for the DSC between radiologist-pulmonologist, radiologist-image analyst and pulmonologist-image analyst was respectively 0.792-0.772, 0.785-0.804 and 0.835-0.857.



2.2.2 Nodule Surface characterization. Nodule shape descriptors such as sphericity, flatness, elongation, spiculation and lobulation are accepted predictors of malignant nodules. We have developed quantitative methods to characterize these features in an automated and reproducible fashion. In addition to these common-place descriptors we also investigated, through a pilot feasibility study, the applicability of unbiased curvature-based shape descriptors. In this approach, the nodule surfaces are meshed, cleaned and smoothed; mean and Gaussian curvatures are computed at the mesh vertices. Based on the vertex-wise signs of the mean and Gaussian curvatures, the vertices are classified into surface features as peak, ridge, saddle ridge, flat, minimal, pit, valley and saddle valley. We showed in our pilot study that unsupervised stratification based on cumulative distribution of these surface features distinguishes benign and malignant nodules. For the pilot study with 90 nodules, we used a disparate set of applications to address the different components of surface characterization (Table 1). This error prone approach took about thirty minutes to process a single nodule. With multiple iterations of this process required during the exploratory stages, it is impractical to process the 657 nodules planned for developing the radiologic model. Therefore we designed, implemented and integrated all the components into a single monolithic software. Due to this significant development effort, the processing time per nodule (excluding the nodule segmentation time) has dramatically reduced to under a second.

Table 1. Algorithmic components of nodule surface characterization and the strategy used during the pilot study and current improvements.

Tools used in Pilot Study	Components	Current Status
ANALYZE	Nodule Segmentation	CANARY-PLUS
ANALYZE AVW	Surface Extraction	In-house monolithic software
ADMESH	Surface Repair	
MATLAB	Surface smoothing	
MeshLab	Discrete Curvatures Estimation	
MATLAB	Surface feature categorization	
CALIPER	Unsupervised clustering	
~ 30 minutes	Time to process one nodule	< 1 second

2.2.3 Development of Score Indicative of Lesion/Lung Aggression/Abnormality (SILA).

Current literature suggests that no single quantitative metric exists to differentiate benign and malignant nodules. However, multivariate predictive models based on an ensemble of nodule texture, surround texture, nodule surface and other shape descriptors could improve the discriminability. To facilitate the multivariate analysis we investigated the possibility of replacing our previously developed nodule texture and surface categorization using unsupervised stratification into continuous variables that can be thresholded at multiple levels to provide, if needed, the necessary categorization. We developed SILA to map the nine nominal texture/surface exemplar distributions of the nodule onto a continuous scale. The nine nominal exemplar distributions can be ordinated in 362,880 (factorial 9) ways. To identify the unique ordination that correlates with the virulence/malignancy of the nodule, we used qualitative spatial reasoning and multi-dimensional scaling. Based on this, the nine texture exemplars arbitrarily labeled as V,I,B,G,Y,O,R,C, and P were ordinated as V-R-O-I-Y-P-B-G-C identical to that used to represent the distributions via the glyphs. The nine surface exemplars were ordinated as unknown-minimal surface-valley-flat-ridge-pit-saddle valley-saddle ridge-peak. SILA was computed as the Cramer-Von Mises Distance of the ordinated exemplar distributions. Using a similar strategy, the seven primal parenchymal exemplars (Normal, Ground Glass,

Honeycombing, Reticular, {mild, moderate, severe} lower attenuation areas) were ordinated to compute the SILA for the parenchyma surrounding the nodule.

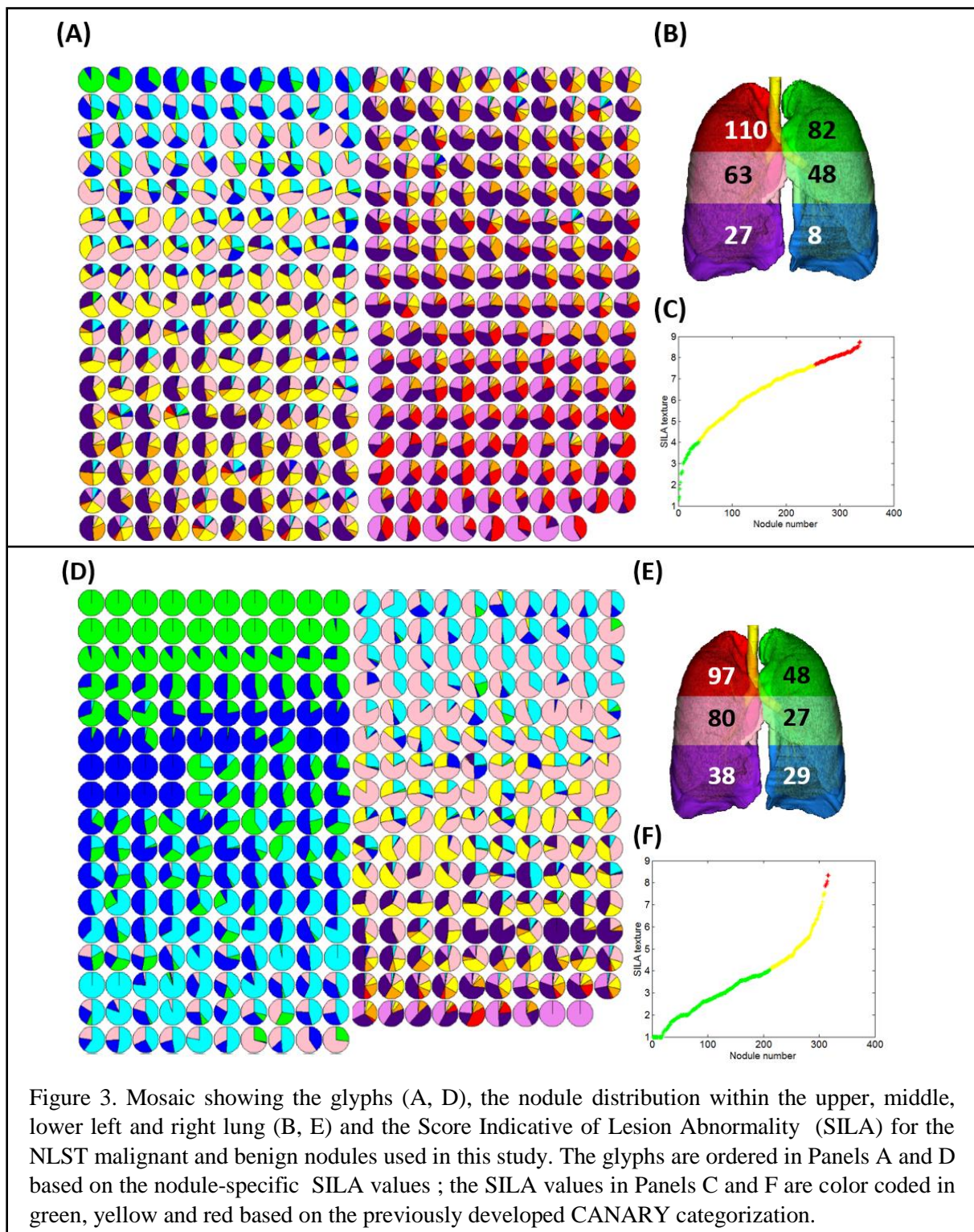
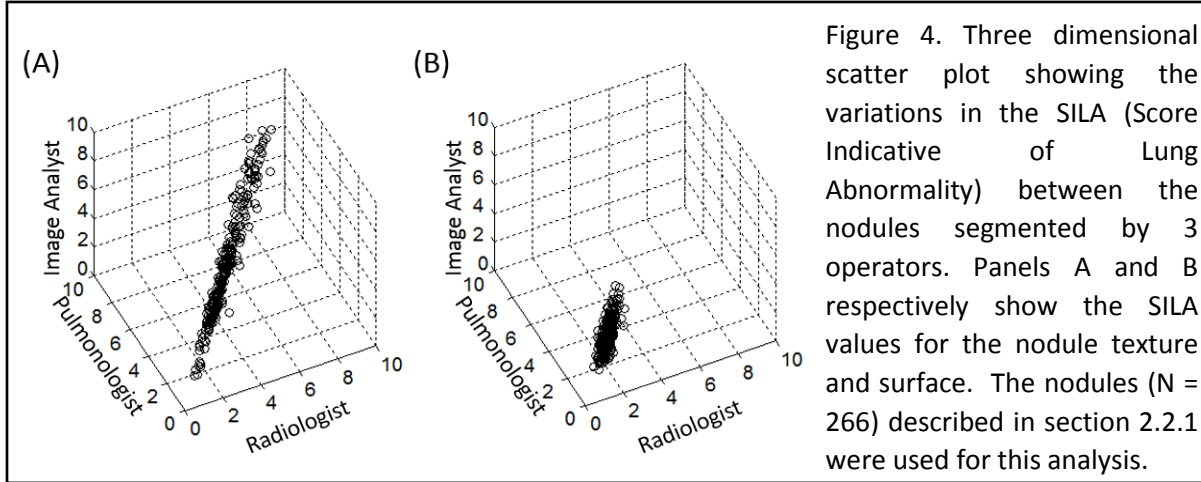


Figure 4 shows the operator dependent variations in the SILA mappings for the texture and surface characterization. The 95% C.I for the maximum nodule-specific SILA differences across the 3 operators was 0.217 – 0.271 and 0.236 – 0.276 respectively for the texture and surface characterization.



2.2.4 Quantitative metrics for the discrimination of benign and malignant lung nodules. A comprehensive number of automatically computable, quantitative metrics were identified for the discrimination of benign and malignant lung nodules (Table 2). These metrics are broadly categorized into

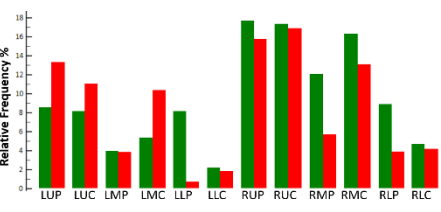
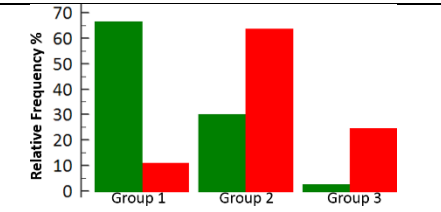
1. Bulk metrics based on the global shape descriptors of the nodule.
2. Intensity metrics based on the CT Hounsfield units within the nodule.
3. Metrics capturing the spatial location of the nodule.
4. Nodule texture metrics based on the CANARY texture exemplar distributions within the nodule.
5. Surround texture metrics based on the parenchymal texture exemplar distributions within a region surrounding the nodule.
6. Metrics capturing the surface descriptors of the nodule.
7. Metrics capturing the distribution of the surface exemplars of the nodule.

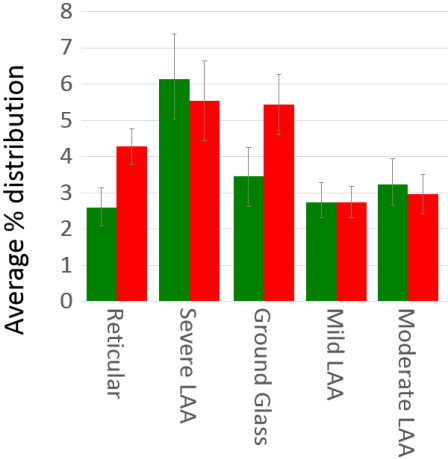
The discriminability of benign and malignant nodules were analyzed using t-test and the normal distribution of the individual metric value was assessed using the quantile-quantile plot and the probability plot correlation coefficient (PPCC). In contradiction to the existing literature, our investigation revealed that skew and kurtosis of the voxel intensities within the nodule is not a discriminator of benign and malignant nodules. This could be attributed to the majority of current work focused on solid nodules.

Table 2. List of quantitative metrics used in the discrimination of benign and malignant nodules. The pval, 95% CI and the probability plot correlation coefficient (PPCC) are given in the last column for benign (N = 319) and malignant (N = 338) nodules.

Metric Category	#	Metric	Description	Pval 95% CI for Benign /Malignant PPCC for Benign/ Malignant
Bulk	1	Volume (V)	Nodule volume in mm ³	< 0.0001 254 – 435 / 2521 – 5716 0.57 / 0.45
	2	Surface Area (S)	Surface in mm ² . Contribution of each surface voxel is determined by the neighbors of that voxel. Additionally, the surfaces which intersect the edge of the volume are included in the measurements.	< 0.0001 289 – 399 / 2479 – 2299 0.71 / 0.61
	3	Sphericity (Sph)	$Sph = \frac{6 * \sqrt{\pi} V}{S^{3/2}}$	< 0.0001 0.57 – 0.63 / 0.48 – 0.53 0.94 / 0.97
	4	Sphere Fit Factor (SFF)	$SFF = \frac{S^3}{\pi(2V/3)^2}$	0.0008 4.63 – 5.92 / 6.3 – 8.18 0.82 / 0.77
	5	Radius (R)	Maximum radius if it were to be spherical nodule . $R = \left(\frac{3V}{4\pi}\right)^{1/3}$	< 0.0001 3.42 – 3.77 / 7.1 – 7.9 0.88 / 0.89
	6	Minimum Enclosing Brick(MEB)	The x,y,z extents of the minimum enclosing brick around the nodule	
	7	MEB Angle	The orientation of the minimum enclosing brick around the nodule	

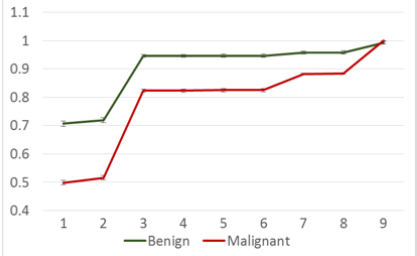
Bulk contd.	8	Elongation (E)	$E = 1.0 - \frac{\varepsilon_{max}}{\varepsilon_{mid}}$ <p>ε_{max}, ε_{mid} are the maximum and middle edge lengths of MEB</p>	0.45 -0.36 – -0.26 / -0.34 – -0.23 0.72 / 0.7
	9	Flatness (F)	$F = 1.0 - \frac{\varepsilon_{mid}}{\varepsilon_{min}}$ <p>ε_{min}, ε_{mid} are the minimum and middle edge lengths of MEB</p>	< 0.0001 -1.12 – -0.89 / 0.68 – -0.46 0.98 / 0.96
Intensity	10	Mean (Avg)	average of the voxel intensities within the nodule	< 0.0001 -487 – -443 / -233 – -195
	11	Variance (Var)	variance the voxel intensities within the nodule	0.06 - .66 / .35
	12	Skew (Skew)	skewness of the voxel intensities within the nodule $Skew = \frac{\sum (x_i - Avg)^3}{N Var^{3/2}}$	0.55 -25 – -2.6 / -3.9 – -1.6 .95 / .42
	13	Kurtosis (Kur)	Kurtosis of the voxel intensities within the nodule $Kur = \frac{\sum (x_i - Avg)^4}{N Var^2}$	0.24 9.43 – 11.64 / -82.34 – 395.39 .68 / .17
	14	Entropy (En)	$En = -x_i * \log_2(x_i)$	< 0.0001 6.57 – 6.96 / 7.47 – 7.88 .68 / .69

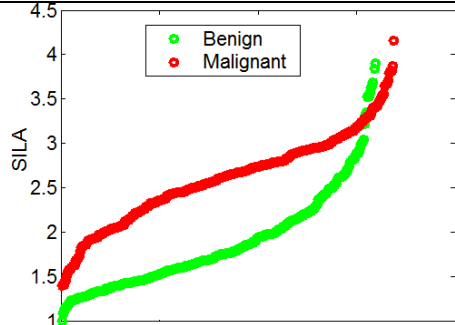
Location	15	Location (Loc)	The Left/Right (L/R), Upper/Middle/Lower (U/M/L), Peripheral / Central (P/C) region containing majority of the nodule voxels. The bar chart on the right shows the relative distribution of the benign (blue) and malignant (red) nodules across the 12 regions.	 <p>PPCV: .97 / .96</p>
	16	Offset from Carina	x,y,z- offsets of the nodule centroid to Carina	
	17	Offset from Hila	x,y,z- offsets of the nodule centroid to Hila	
	18	Offset from Pleura	x,y,z- offsets of the nodule centroid to Pleura	
Nodule Texture	19	Exemplar Distribution	Distribution of the nine CANARY texture exemplars constituting the nodule	
	20	SILA	Score Indicative of Lesion Aggression for the nodule texture.	<p>< 0.0001</p> <p>54.42 – 62.81 / 116.88 – 124.58</p> <p>0.98 / 0.97</p>
	21	Risk Category	Risk Stratification group. The bar chart on the right shows the relative distribution of the risk groups for benign (green) and malignant (red) nodules.	 <p>PPCV: .8 / .87</p>

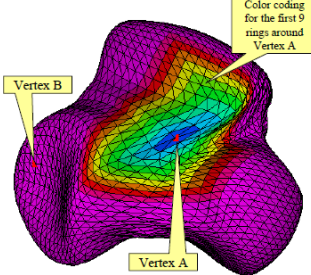
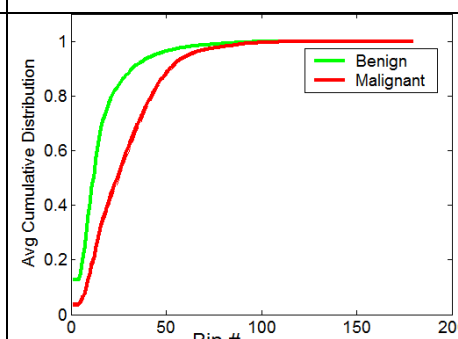
Nodule Surround Texture	22	Surround Distribution	Distribution of the 7 parenchymal exemplars (Normal, Honey comb, Reticular, Ground glass, mild low attenuation area (LAA , moderate LAA, severe LAA) within 10 mm around the nodule. Bar chart on the right shows the average % distribution of non-normal exemplars for the benign (green) and red (malignant) nodules	
	23	Percentage Vessels	Percentage of Vessels within a 10 mm region around the nodule	< 0.0001 0.61 – 0.89 / 1.41 – 1.77 0.8 / 0.91
	24	Percentage Background	Percentage of non-lung voxels around the nodule	0.928 8.35 – 10.81 / 8.65 – 10.68 0.9 / 0.94
	25	SILA_Fib	SILA score for the distribution of honey comb, reticular and ground glass surrounding the nodule.	0.001 24.89 – 29.95 / 30.62 – 34.48 0.96 / 0.99
	26	SILA_LAA	SILA score for the distribution of mild, moderate and severe LAA.	0.05 30.5 – 34.88 / 33.62 – 37.2 0.98 / 0.99
Nodule Surface	27	Number of Vertices NV	Number of vertices in the surface	< 0.0001 438 – 592 / 2262 – 3373 0.72 / 0.63
	28	Willmore Bending Energy (WEB)	Given the per-vertex principal curvatures k_1 and k_2 , $WEB = \int_A (k_1^2 + k_2^2) dA$	< 0.0001 401 – 560 / 1377 – 2279 0.72 / 0.57
	29	H: Min		< 0.0001 -0.33– -0.23 / -1.05 – -0.90 0.89 / 0.97

Nodule Surface contd.	30	H: Max	<p>Mean curvature (H) is an extrinsic curvature that arises from the mechanical folding of the surface.</p> $H = \frac{(k_1 + k_2)}{2}$	< 0.0001 3.07 – 3.47 / 3.82 – 4.45 0.84 / 0.87
	31	H: -ve Avg		0.2 -0.14 – -0.12 / -0.15 – -0.13 - / -
	32	H: +ve Avg		< 0.0001 0.56 – 0.60 / 0.35 – 0.37 0.98 / 0.94
	33	H: -ve Skew		< 0.0001 -1.1 – -0.85 / -2.2 – -1.97 - / -
	34	H: +ve Skew		< 0.0001 1.88 – 2.14 / 2.97 – 3.44 0.98 / 0.94
	35	G: Min	<p>Gaussian Curvature (G)</p> $G = k_1 * k_2$	0.0005 -0.96 – -0.78 / -1.21 – -1.01 0.86 / 0.88
	36	G: Max		0.0004 10.27 – 14.93 / 17.41 – 26.62 0.6 / 0.64
	37	G: -ve Avg		0.30 -93 – 30.21 / -0.06 – -0.055 0.16 / 0.86
	38	G: +ve Avg		< 0.0001 0.56 – 0.67 / 0.31 – 0.44 0.84 / 0.61
	39	G: -ve Skew		< 0.0001 -2.52 – -2.2 / -4.46 – -4.0 - / -
	40	G: +ve Skew		< 0.0001 4.43 – 4.9 / 7.41 – 8.21 0.94 / 0.96

Nodule Surface contd.	41	Sharpness (S): Min	<p>Sharpness at a vertex emphasizes regions where k_1 and k_2 are maximally different as in the crests and depths.</p> $S_i = (k_1^2 - k_2^2)$	< 0.0001 $-0.8 - -0.64 / -1.6 - -1.4$ $0.95 / 0.98$
	42	S: Max		< 0.0001 $3.56 - 4.16 / 5.12 - 5.96$ $0.85 / 0.91$
	43	S: Avg		< 0.0001 $0.65 - 0.70 / 0.39 - 0.42$ $0.98 / 0.97$
	44	S: Skew		< 0.0001 $1.1 - 1.34 / 1.65 - 2.01$ $0.94 / 0.91$
	45	Curvedness (C): Min	<p>Curvedness captures information on less sharp folding thus revealing smaller bumps and ridges.</p> $C = \sqrt{\left(\frac{k_1^2 + k_2^2}{2}\right)}$	< 0.0001 $0.03 - 0.04 / 0.003 - 0.005$ $0.88 / 0.87$
	46	C: Max		< 0.0001 $2.35 - 2.68 / 3.10 - 3.63$ $0.83 / 0.89$
	47	C: Avg		< 0.0001 $0.47 - 0.51 / 0.30 - 0.32$ $0.98 / 0.94$
	48	C: Skew		< 0.0001 $1.71 - 1.99 / 2.94 - 3.46$ $0.90 / 0.87$
	49	Shape Index (SI): Min	$SI = \frac{2}{\pi} \tan^{-1} \left(\frac{k_1 + k_2}{k_2 - k_1} \right)$	< 0.0001 $-0.62 - -0.48 / -0.1 - -0.96$ $0.81 / 0.33$
	50	SI: Max		< 0.0001 $0.975 - 0.978 / 0.982 - 0.984$ $0.91 / 0.94$
	51	SI: Avg		< 0.0001 $0.54 - 0.56 / 0.28 - 0.31$ $0.97 / 0.99$

Nodule Surface contd.	52	SI: Skew		0.5 -1.87 – -1.56 / -1.75 – -1.56																														
	53	Intrinsic Curvature Index (ICI)	ICI counts the number of regions with undulations or saliencies on the surface. $ICI = \frac{1}{4\pi} \iint k_{min} k_{max} dA$ where $k_{min} = H - \sqrt{H^2 - G}$ $k_{max} = H + \sqrt{H^2 - G}$	< 0.001 13.33 – 18.08 / 34.94 – 64.15 0.72 / 0.81																														
	54	Extrinsic Curvature Index (ECI)	ECI counts the number and length (with respect to the diameter) cracks and gaps on the surface. $ECI = \frac{1}{4\pi} \iint k_{mzx} (k_{max} - k_{min}) dA$	< 0.0001 33.13 – 45.7 / 100.2 – 167.8 0.71 / 0.82																														
Morpheme	55	Morpheme Distribution	The distribution of the nine morphometric exemplars of the nodule surface. The plot on the right shows the average cumulative distribution between the benign (green) and malignant (red) nodules.	 <table><caption>Cumulative Distribution Data (Estimated from Graph)</caption><thead><tr><th>Exemplar</th><th>Benign</th><th>Malignant</th></tr></thead><tbody><tr><td>1</td><td>0.70</td><td>0.50</td></tr><tr><td>2</td><td>0.72</td><td>0.52</td></tr><tr><td>3</td><td>0.95</td><td>0.82</td></tr><tr><td>4</td><td>0.95</td><td>0.82</td></tr><tr><td>5</td><td>0.95</td><td>0.82</td></tr><tr><td>6</td><td>0.95</td><td>0.82</td></tr><tr><td>7</td><td>0.96</td><td>0.88</td></tr><tr><td>8</td><td>0.97</td><td>0.90</td></tr><tr><td>9</td><td>1.00</td><td>1.00</td></tr></tbody></table>	Exemplar	Benign	Malignant	1	0.70	0.50	2	0.72	0.52	3	0.95	0.82	4	0.95	0.82	5	0.95	0.82	6	0.95	0.82	7	0.96	0.88	8	0.97	0.90	9	1.00	1.00
Exemplar	Benign	Malignant																																
1	0.70	0.50																																
2	0.72	0.52																																
3	0.95	0.82																																
4	0.95	0.82																																
5	0.95	0.82																																
6	0.95	0.82																																
7	0.96	0.88																																
8	0.97	0.90																																
9	1.00	1.00																																

Morpheme contd.	56	SILA Morpheme	Score Indicative of Lesion Abnormality based on the morpheme distribution. The plot on the right shows the distribution of SILA morpheme for benign and malignant nodules	 <p>< 0.0001 1.81 – 1.94 / 2.55 – 2.66 0.95 / 0.99</p>		
	57	Morpheme Curvedness (MC): Avg	Morpheme-wise average curvedness of the surface. The table to the right shows the pvals and 95% CI for the benign and malignant nodules. Sig = Significant (< 0.0001); NS = not significant	Id	p	95% CI
			1	Sig	0.52 – 0.56 / 0.39 – 0.41	
			2	NS	0.007– 0.03 / 0.008– 0.17	
			3	Sig	0.4 – 0.44 / 0.26 – 0.28	
			4	-		
			5	-		
			6	-		
			7	NS	0.21 – 0.26 / 0.2 – 0.23	
			8	NS	0.01 – 0.04 / 0.01 – 0.02	
		9	Sig	0.2 – 0.23 / 0.15 – 0.16		
58	MC: Skew	Morpheme-wise skew of curvedness of the surface. The table to the right shows the pvals and 95% CI for the benign and malignant nodules	Id	p	95% CI	
		1	Sig	1.51 – 1.73 / 2.38 – 2.76		
		2	0.02	2.6 – 3.8 / 3.75 – 4.59		
		3	Sig	1.04 – 1.31 / 2.15 – 2.54		
		4	-			
		5	0.32	0.46 – 2.33 / 1.45 – 8.7		
		6	-			
		7	Sig	0.33 – 0.57 / 1.21 – 1.41		
		8	0.07	0.21 – 1.7 / 1.6 – 2.4		
		9	Sig	0.49 – 0.71 / 1.32 – 1.52		

Morpheme contd.	59	Local SILA : Avg	Local morpheme SILA was computed by finding 2-ring neighbors around each vertex. The figure below shows the color coded 9-ring neighbor around a sample vertex for a representative	< 0.0001 14.38 – 16.32 / 26.74 – 28.64 0.95 / 0.99
	60	Local SILA: Skew	 <p>nodule.</p> <p>The average and skew of the local SILA distribution was computed.</p>	< 0.0001 0.41 – 0.56 / 0.66 – 0.75 0.99 / 0.99
	61	Local SILA: Histogram	Figure to the right shows the average cumulative distribution of the local morpheme SILA for the benign and malignant nodules	

2.2.5 Decision tree based approach for the discrimination of benign and malignant lung nodules. During the investigation, we observed that a number of benign nodules in the NLST cohort were flat and much smaller than 7 mm in diameter. On the contrary, all the malignant nodules were above 7 mm. To prevent contamination of the radiologic model by these tiny nodules we used a decision tree based approach (Figure 5) to facilitate the robust discrimination of benign and malignant nodules. Size filter was based on the maximal extent of the minimum enclosing brick edge lengths. Flatness check was based on the number of transverse sections covering the nodule. Using these criteria, 128 of the 319 benign nodules were eliminated from the subsequent radiologic modeling; none of the 338 malignant nodules met the criteria and were all used in the modeling. Candidate metrics for the radiologic model was selected using the ROC analysis of the individual metrics. Metrics with AUC values above 0.75 (shown highlighted in

Table 3) were selected as candidates for the radiologic modeling which is currently being pursued. Models based on Linear/Quadratic discriminant analysis, multinomial logistic regression and support vector machines are being investigated.

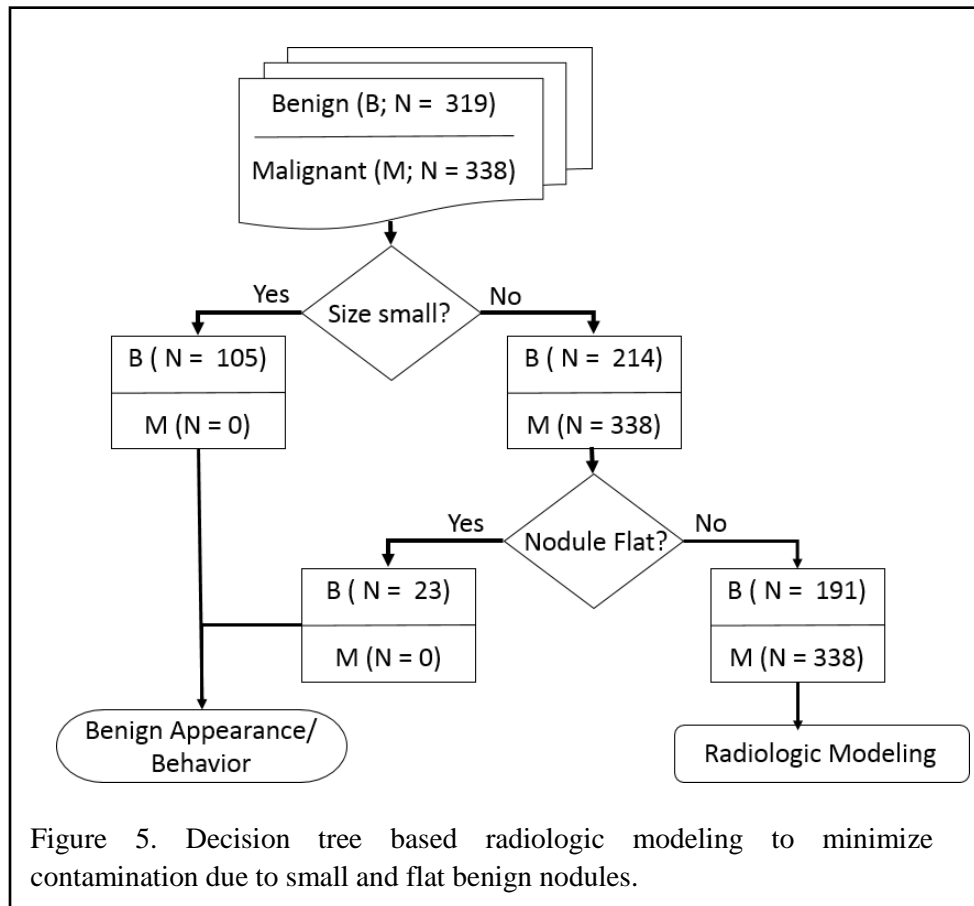


Table 3. ROC analysis of the nodule metrics to identify the potential candidates of the radiologic modeling. Using an arbitrary cut-off of 0.75 for AUC, 14 metrics (highlighted in the table) were selected as candidate metrics.

#	Metric	AUC	SE	95% CI
1	Volume	0.84	0.0181	0.804 to 0.875
2	Surface Area	0.803	0.0197	0.764 to 0.841
3	Sphericity	0.569	0.0255	0.519 to 0.619
4	Sphere Fit Factor	0.569	0.0255	0.519 to 0.619
5	Estimated Radius	0.840	0.0181	0.804 to 0.875
6	Elongation	0.570	0.0255	0.520 to 0.620
7	Flatness	0.635	0.0255	0.585 to 0.685
8	HU_mean	0.810	0.0193	0.77 to 0.848
9	HU_variance	0.544	0.0258	0.493 to 0.594
10	HU_skew	0.539	0.0249	0.490 to 0.587

11	HU_kurtosis	0.709	0.0226	0.664 to 0.753
12	HU_entropy	0.705	0.0231	0.659 to 0.750
13	Location	0.570	0.0257	0.519 to 0.620
14	SILA Texture	0.838	0.0186	0.802 to 0.875
15	Texture Risk	0.762	0.0221	0.719 to 0.805
16	Vessels %	0.677	0.0251	0.628 to 0.726
17	Background %	0.543	0.0272	0.489 to 0.596
18	SILA_Fibrosis	0.588	0.0277	0.534 to 0.642
19	SILA_LAA	0.568	0.0274	0.514 to 0.621
20	Number of Vertices	0.815	0.0189	0.778 to 0.852
21	Willmore Bending energy	0.699	0.0232	0.654 to 0.745
22	Min Mean Curvature	0.735	0.0223	0.691 to 0.745
23	Max Mean Curvature	0.551	0.0254	0.501 to 0.6
24	Avg -ve Mean Curvature	0.509	0.0276	0.455 to 0.563
25	Avg +ve Mean Curvature	0.775	0.0218	0.732 to 0.818
26	Skew +ve Mean Curvature	0.652	0.0242	0.604 to 0.6999
27	Min Gaussian Curvature	0.585	0.0265	0.533 to 0.637
28	Max Gaussian Curvature	0.544	0.0256	0.494 to 0.594
29	Avg -ve Gaussian Curvature	0.722	0.0248	0.673 to 0.770
30	Skew -ve Gaussian Curvature	0.740	0.023	0.695 to 0.785
31	Avg +ve Gaussian Curvature	0.674	0.0246	0.626 to 0.722
32	Skew +ve Gaussian Curvature	0.728	0.0222	0.685 to 0.772
33	Min Sharpness	0.656	0.0245	0.608 to 0.704
34	Max Sharpness	0.603	0.0253	0.553 to 0.652
35	Avg Sharpness	0.796	0.0201	0.756 to 0.835
36	Skew Sharpness	0.585	0.0259	0.535 to 0.636
37	Min Curvedness	0.753	0.0233	0.707 to 0.799
38	Max Curvedness	0.564	0.0253	0.514 to 0.613
39	Avg. Curvedness	0.780	0.0216	0.738 to 0.822
40	Skew Curvedness	0.654	0.0242	0.607 to 0.702
41	Min Shape Index	0.735	0.0223	0.691 to 0.778
42	Max Shape Index	0.621	0.0252	0.571 to 0.670
43	Avg Shape Index	0.807	0.0189	0.770 to 0.844
44	Skew Shape Index	0.724	0.0236	0.677 to 0.770
45	ICI	0.637	0.0245	0.589 to 0.686
46	ECI	0.685	0.0236	0.639 to 0.732
47	SILA Texture	0.775	0.0222	0.731 to 0.818
48	Avg Curvature T1	0.704	0.0235	0.657 to 0.750
49	Avg_Curvature_T3	0.772	0.0214	0.730 to 0.814
50	Avg_Curvature_T9	0.586	0.0295	0.529 to 0.644
51	Skew Curvature_T1	0.642	0.0246	0.594 to 0.726
52	Avg Local SILA	0.776	0.0218	0.733 to 0.819
53	Skew Local SILA	0.510	0.0273	0.457 to 0.564

2.3 Development of a radiologic and clinical/radiologic prediction model:

Due to delays in establishing subcontracts with Mayo Clinic and Brown University, this sub aim has not been started yet.

2.4 Validation of a radiologic and clinical/radiologic prediction model:

This aim is scheduled to start in the 2nd year of the grant.

3. What opportunities for training and professional development has the project provided?

Nothing to report

4. How were the results disseminated to communities of interest?

Nothing to report

5. What do you plan to do during the next reporting period to accomplish these goals?

The development and optimization of different quantitative radiological variables has just been completed. The most promising variables as determined by receiver operative characteristics (ROC) curve analysis have been identified and will be combined by using multivariate logistic regression analysis, linear/quadratic discriminant analysis, support vector machines into a radiologic predictive model. The performance of this radiologic predictive model will be assessed by ROC curve analysis. We anticipate being able to generate this model by December 2016. Clinical and epidemiologic variables known to be predictive of malignancy (such as smoking status, age, known emphysema, etc...) available from the NLST database will then be combined with the radiologic variables to derive a combined radiologic/clinical predictive model using multivariate logistic regression. The performance of this model will be assessed using ROC curve analysis. We anticipate this combined model to be developed before the end of the calendar year 2016.

Year 2 of the grant will be dedicated to validating these two models using the DECAMP-1 dataset.

3. IMPACT

1. What was the impact on the development of the principal discipline(s) of the project?

An estimated 1.5 million new lung nodules are identified via chest CT annually in the US. This is likely to increase with the implementation of lung cancer screening for high-risk individuals. An estimated 10 million individuals in the US are eligible for screening. A significant proportion of these individuals are US veterans, disproportionately affected by tobacco use and other exposures. Results from the NLST suggest that annual screening via low-dose CT results in a 20% relative reduction in lung cancer mortality. However, the large number of false positive screening CTs, 27% in the NLST, are likely to lead to unnecessary invasive diagnostic

interventions and treatments exposing screened individuals to excessive morbidity, mortality, stress and healthcare expenses.

Currently lung nodules are evaluated by radiologists and the probability of malignancy based on subjective interpretations relying on features known to be predictive of lung cancer (such as size and shape of the nodule). With modern CT machines however, a considerable amount of data is available and are not currently exploited. Each nodule is composed of a considerable amount of voxels (similar to pixels, but in 3 dimensions) with variable density values. We have shown in our prior work that these data could be used to non-invasively risk-stratify nodules of the main subgroup of lung cancer: lung adenocarcinoma. In this project, we are using similar quantitative analytics to provide radiologists with objective non-invasive assessment of the likelihood for a nodule to be benign or malignant. Our data are very encouraging and suggest that this may be an attainable goal. If confirmed and validated on an independent cohort of indeterminate lung nodules, as we are planning to do in year 2 of this grant, this novel technology could revolutionize lung nodule management and mitigate the risks inherent in indiscriminate implementation of mass lung cancer screening.

2. What was the impact on other disciplines?

Nothing to report

3. What was the impact on technology transfer?

Nothing to report

4. What was the impact on society beyond science and technology?

If successful, our project could lead to a widely available platform available to clinicians and radiologists that could facilitate the management of screen- or incidentally identified lung nodules, a major healthcare issue for Veteran and non-Veteran populations at risk. Quantitative nodule analysis can be applied to existing CT scans obtained for screening or clinical indications and do not require additional testing beyond application of image analytics. Our quantitative analytics tool could help standardize the management of lung nodules and lead to a substantial reduction in the unnecessary morbidity, mortality and healthcare costs associated with the current paradigm.

5. CHANGES/PROBLEMS

1. Changes in approach and reasons for change:

Our preliminary data presented in the narrative in the project narrative of the grant suggested that quantitative nodule characteristics that could provide valuable information on the benign or malignant character of a nodule would belong to one of the 6 following categories: density-based signatures, characteristics of the tumor-free surrounding lung, nodule morphometrics (i.e. nodule surface analysis), and nodule volume, location and counts.

Nodule location and counts can easily be ascertained without recourse to sophisticated quantitative analytical algorithms and immediately available from the radiology report of the CT scan. Hence, it was decided to include these variables as part of the clinical and epidemiological variables that will be combined with radiological quantitative variables as part of the combined radiologic/clinical predictive model.

2. Actual or anticipated problems or delays and actions or plans to resolve them:

While the award was effective on September 30, 2015, because of relocation of the grant PI from Mayo Clinic, Rochester, MN to Vanderbilt University, Nashville, TN, subcontracts had to be established between the three partnering institutions (Mayo Clinic, Brown University and Vanderbilt University) and were only finalized in April 2016. This resulted in a significant delay for case selection and image transfer from the ACRIN and LSS core labs and our work on the development and optimization of discriminative radiological quantitative variables. While this initial step has nearly been completed, the integration of the variables into multivariate radiologic and combined clinical/radiologic predictive models was accordingly delayed. We anticipate being able to derive these models before the end of the calendar year 2016. In parallel, we initiated the process of image transfer from the DECAMP1 dataset and started preparing the database in a blinded fashion for future analysis by our predictive models. We therefore anticipate being able to complete our project within the timeframe allowed by the grant.

3. Changes that had a significant impact on expenditures

Nothing to report.

4. Significant changes in use or care of human subjects, vertebrate animals, biohazards, ad/or select agents

Nothing to report

6. PRODUCTS

1. Publications, conference papers, and presentations

Nothing to report

2. Website(s) or other internet site(s)

Nothing to report

3. Technologies or techniques

Novel CT-based quantitative analytics to distinguish benign from malignant nodules. How this novel analytical tools will be shared has not yet been determined.

4. Inventions, patent applications and/or licenses

Nothing to report

5. Other products

Nothing to report

7. PARTICIPANTS & OTHER COLLABORATING ORGANIZATIONS

Name: Tobias Peikert

Project Role: PD/PI

Research Identifier: N/A

Nearest Person Months: 1.0

Contribution to the Project: Mayo Clinic PI, administrative leadership at Mayo Clinic, review and selection of all benign NLST (nodules) training set and benign and malignant DECAMP nodules. Shared supervision of Dr. Rajagopalan and Ron Karwoski with Dr. Bartholmai.

Participation in weekly team videoconferences.

Name: Brian Bartholmai

Project Role: Co-Investigator

Research Identifier: 0000-0001-7834-6579

Nearest Person Months: 1.0

Contribution to the Project: Radiology leader and liaison to DECAMP team. Selection all technically appropriate DCAMP scans and selection of all benign NLST (nodules) training set and benign and malignant DECAMP nodules. Shared supervision of Dr. Rajagopalan and Ron Karwoski with Dr. Peikert. Participation in weekly team videoconferences.

Name: Srinivasan Rajagopalan

Project Role: Co-Investigator

Research Identifier: [0000-0003-3286-1529](#)

Nearest Person Months: 6.0

Contribution to the Project: Image analysis and development of imaging variables. Participation in weekly meetings.

Name: Fenghai Duan, PhD

Project Role: CSS subcontract PI

Researcher Identifier: 306213

Nearest person months worked: 1.2 CM

Contribution to project: This 2-year subcontract officially started in the beginning of 2016. Erin and Fenghai are working with the investigators to design the study, establish and support access to the clinical data and images of NLST and DECAMP, develop database linking clinical and radiological data for study analysis, develop analysis plan, and address methodological issues arising in the design and analysis, etc. To date, they have developed the plan and delivered the required clinical and radiological data to the Mayo Clinic.

Name: Erin Greco, MS

Project Role: Biostatistician

Researcher Identifier: 315034

Nearest person months worked: 1.38 CM

Contribution to project: This 2-year subcontract officially started in the beginning of 2016. Erin and Fenghai are working with the investigators to design the study, establish and support access to the clinical data and images of NLST and DECAMP, develop database linking clinical and radiological data for study analysis, develop analysis plan, and address methodological issues arising in the design and analysis, etc. To date, they have developed the plan and delivered the required clinical and radiological data to the Mayo Clinic.

Other Support Changes (since initial application)

Maldonado, Fabien, M.D.

Ended: EP00068928 CHEST Foundtion and Boehringer Ingelheim (Maldonado); CLN0009-01.p.B-1 PneumRx, Inc. (Maldonado)

New: Centurion Medical Products (Maldonado)

Duan, Fenghai, Ph.D.

Ended: U10 CA 079778 (Gatsonis)

New: U01 CA 190254 (Schnall); U01 CA 196408 (Dubinett); American College of Radiology (ACR) Schnall; Blue Earth Diagnostics (Duan)

Bartholmai, Brian, M.D.

Ended: none

New: R01 HL 125234 (Zhang); LAM0110P03-15 (Bartholmai)

Srinivasan, Rajagopalan, Ph.D.

Ended: None

New: LAM0110P03-15 (Bartholmai)

Tobias, Peikert, M.D.

Ended: K23 CA 159391 (Peikert)

New: Career Dev. Award – Walter & Leonore Annenberg (Peikert)

8. SPECIAL REPORTING REQUIREMENTS

None

9. APPENDICES